

ROBUST SOFT-CONSTRAINED SPATIALLY SELECTIVE ACTIVE NOISE CONTROL FOR HEARABLES UNDER SECONDARY PATH VARIATIONS

Tong Xiao¹, Reinhild Roden², Matthias Blau², Simon Doclo¹

¹ Department of Medical Physics and Acoustics and Cluster of Excellence “Hearing4all.connects”,
Carl von Ossietzky Universität Oldenburg, Germany
tong.xiao@uni-oldenburg.de, simon.doclo@uni-oldenburg.de

² Institut für Hörtechnik und Audiologie and Cluster of Excellence “Hearing4all.connects”,
Jade-Hochschule, Oldenburg, Germany
reinhild.roden@jade-hs.de, matthias.blau@jade-hs.de

ABSTRACT

Spatially selective active noise control (SSANC) hearables aim to attenuate noise from certain directions at the eardrum while preserving desired speech arriving from selected directions. Existing SSANC systems typically assume an accurate estimate of the secondary path from the loudspeaker to the inner error microphone. In practice, however, this path varies across users and device fits, which can degrade performance and compromise system stability. This paper proposes a robust soft-constrained optimization framework that computes a single control filter by minimizing the average cost over a set of secondary path estimates derived from human measurements. Simulations and experiments on a real-time control platform show that the proposed approach slightly reduces mean performance relative to the matched case but substantially narrows the performance spread under secondary path mismatch. The proposed framework therefore provides a practical design strategy when accurate secondary path estimates are unavailable.

Index Terms— Active noise control, spatially selective active noise control, soft constraints, secondary path variations, hearables

1. INTRODUCTION

Active noise control (ANC) hearables use secondary sources to generate anti-noise to minimize the noise leakage at the eardrum [1–3]. Conventional ANC hearables treat all incoming sounds as noise [4, 5]. This becomes problematic in complex acoustic environments when desired speech is present [6–11]. In these cases, the user may want to focus on a specific speech source from a certain direction (e.g., the front) while reducing the noise leakage from other directions.

To achieve this, modern hearables employ a combination of outer microphones and inner error microphones. While traditional beamforming methods preserve desired speech, they often ignore the leakage at the inner error microphones [12–14]. Spatially selective ANC (SSANC) combines beamforming and ANC principles to preserve speech from desired directions while reducing noise from other directions [11, 15, 16]. A soft-constrained SSANC system was recently proposed to use a trade-off parameter to balance the noise reduction and speech distortion [17]. So far, these approaches have assumed an accurate secondary path estimate between the secondary source and the inner error microphone. In practice, these paths vary

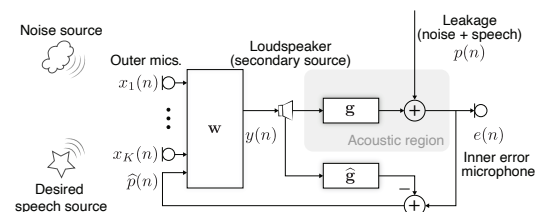


Fig. 1. Block diagram of an SSANC system with K outer microphones, one inner error microphone and one loudspeaker (i.e., secondary source). The control filter is denoted by \mathbf{w} , the secondary path is denoted by \mathbf{g} , and its estimate by $\hat{\mathbf{g}}$.

across individuals due to ear anatomy and device fit. Such mismatches can degrade performance and compromise system stability.

In this paper, we propose a robust optimization framework for soft-constrained SSANC under secondary path variations. We assume that a set of secondary path estimates is available to represent variations across different users and device fittings when the exact secondary path is unknown. Instead of estimating a specific individual path, we determine a control filter that is robust to secondary path variations by minimizing the average cost function evaluated over this set of estimates. A similar robust optimization was recently proposed for sound pressure equalization [18]. For experimental validation, we implemented the proposed framework in real time using a dSPACE SCALEXIO LabBox system. The experimental results are consistent with the simulation findings. This framework provides a practical design option for hearables when accurate secondary path estimation is unavailable.

2. SIGNAL MODEL

As shown in Fig. 1, we consider a hearable with K outer microphones. Without loss of generality, we consider one loudspeaker as the secondary source and one inner error microphone, resulting in a total of $K + 1$ microphones. We assume that the acoustic feedback paths between the loudspeaker and the outer microphones are known, such that acoustic feedback can be canceled.

The inner error microphone signal $e(n)$, with n the discrete time index, is given by

$$e(n) = p(n) + (\mathbf{G}\mathbf{w})^T \mathbf{x}(n), \quad (1)$$

where $(\cdot)^T$ denotes the transpose operator. The leakage (including noise and desired speech) at the inner error microphone is denoted by $p(n)$, and the anti-noise component at the inner error microphone

This research was funded by the Deutsche Forschungsgemeinschaft (DFG, German Research Foundation) – Project-ID 352015383 – SFB 1330 C1, and Germany’s Excellence Strategy – EXC 2177/2 – Project ID 390895286.

is given by $(\mathbf{G}\mathbf{w})^T \mathbf{x}(n)$, where \mathbf{w} is the stacked control filter, $\mathbf{x}(n)$ is the stacked input vector, and \mathbf{G} represents the secondary path convolution matrix. The stacked control filter \mathbf{w} is defined as

$$\mathbf{w} = [\mathbf{w}_1^T \quad \mathbf{w}_2^T \quad \dots \quad \mathbf{w}_{K+1}^T]^T \in \mathbb{R}^{(K+1)L_w}, \quad (2a)$$

$$\mathbf{w}_k = [w_{k,0} \quad w_{k,1} \quad \dots \quad w_{k,L_w-1}]^T \in \mathbb{R}^{L_w}, \quad (2b)$$

where L_w denotes the control filter length for each channel. The convolution matrix of the secondary path $\mathbf{g} = [g_0 \quad g_1 \quad \dots \quad g_{L_g-1}]^T$ with a length of L_g is defined as

$$\mathbf{G} = \text{blkdiag}(\mathbf{G} \dots \mathbf{G}) \in \mathbb{R}^{(K+1)L \times (K+1)L_w}, \quad (3a)$$

$$\mathbf{G} = \begin{bmatrix} g_0 & \dots & 0 \\ \vdots & \ddots & \vdots \\ g_{L_g-1} & \dots & g_0 \\ \vdots & \ddots & \vdots \\ 0 & \dots & g_{L_g-1} \end{bmatrix} \in \mathbb{R}^{L \times L_w}, \quad (3b)$$

where $L = L_g + L_w - 1$. As input signals to the control filter, we consider the K outer microphone signals $\mathbf{x}_k(n)$, $k = 1, \dots, K$, and an estimate of the leakage $\hat{\mathbf{p}}(n)$. The stacked input vector $\mathbf{x}(n)$ is defined as

$$\mathbf{x}(n) = [\mathbf{x}_1^T(n) \quad \dots \quad \mathbf{x}_K^T(n) \quad \hat{\mathbf{p}}^T(n)]^T \in \mathbb{R}^{(K+1)L}, \quad (4)$$

with

$$\mathbf{x}_k(n) = [x_k(n) \quad \dots \quad x_k(n-L+1)]^T \in \mathbb{R}^L, \quad (5a)$$

$$\hat{\mathbf{p}}(n) = [\hat{p}(n) \quad \dots \quad \hat{p}(n-L+1)]^T \in \mathbb{R}^L. \quad (5b)$$

The estimated leakage $\hat{\mathbf{p}}(n)$ can be computed from the inner error microphone signal $e(n)$, the loudspeaker signal vector $\mathbf{y}(n) = [y(n) \quad \dots \quad y(n-L_g+1)]^T$, and an estimate of the secondary path $\hat{\mathbf{g}} = [\hat{g}_0 \quad \hat{g}_1 \quad \dots \quad \hat{g}_{L_g-1}]^T \in \mathbb{R}^{L_g}$ as

$$\hat{\mathbf{p}}(n) = e(n) - \hat{\mathbf{g}}^T \mathbf{y}(n). \quad (6)$$

To derive the optimal control filter, we first assume an accurate secondary path estimate, $\hat{\mathbf{g}} = \mathbf{g}$. Under this assumption, the estimated leakage equals the true leakage, $p(n) = \hat{p}(n) = \mathbf{q}^T \mathbf{x}(n)$, with

$$\mathbf{q} = [\mathbf{0}^T \quad \dots \quad \mathbf{0}^T \quad \delta^T]^T \in \mathbb{R}^{(K+1)L}, \quad (7a)$$

$$\delta = [1 \quad 0 \quad \dots \quad 0]^T \in \mathbb{R}^L. \quad (7b)$$

Hence, the inner error microphone signal in (1) can be rewritten as

$$e(n) = (\mathbf{q} + \mathbf{G}\mathbf{w})^T \mathbf{x}(n). \quad (8)$$

While this assumption is used to derive the optimal control filter, the true secondary path can vary for different individuals and for different device fits. This mismatch can cause the estimated leakage to differ from the true leakage, which impacts the system performance. However, we first establish a matched-case performance reference before analyzing secondary path mismatch.

3. SSANC FORMULATION AND EVALUATION CASES

The objective of the SSANC system is to minimize the power of the inner error microphone signal while preserving the delayed desired speech component of an outer reference microphone signal. A soft-constrained optimization has been proposed to balance the noise reduction and the speech distortion [17]. The cost function is formulated as

$$\min_{\mathbf{w}} \mathcal{E}\{e^2(n)\} + \mathbf{w}^T \mathbf{B}\mathbf{w} + \mu \|\mathbf{H}(\mathbf{q} + \mathbf{G}\mathbf{w}) - \alpha \delta_{\Delta}\|_2^2, \quad (9)$$

where $\mathcal{E}\{\cdot\}$ denotes the mathematical expectation operator. $\mathbf{w}^T \mathbf{B}\mathbf{w}$ is a regularization term to prevent overloading the secondary source and to ensure stability, with \mathbf{B} being a block-diagonal matrix applying different penalty weights to the feedforward (FF) and feedback (FB) channels. It is defined as

$$\mathbf{B} = \text{blkdiag}(\beta_{\text{FF}}\mathbf{I}, \dots, \beta_{\text{FF}}\mathbf{I}, \beta_{\text{FB}}\mathbf{I}) \in \mathbb{R}^{(K+1)L_w \times (K+1)L_w}, \quad (10)$$

where β_{FF} and β_{FB} are the regularization parameters for the FF and FB channels, respectively, and \mathbf{I} denotes the $L_w \times L_w$ identity matrix. The real-valued positive parameter μ controls the trade-off between noise reduction and speech distortion. A larger μ emphasizes speech preservation, while a smaller μ allows for more noise reduction at the cost of increased speech distortion. The matrix \mathbf{H} contains the acausal relative impulse responses (ReIRs), and δ_{Δ} represents the delayed target response with a delay of Δ samples [15, 16],

$$\mathbf{H} = [\mathbf{H}_1 \quad \dots \quad \mathbf{H}_{K+1}] \in \mathbb{R}^{(L_a+L_h+L-1) \times (K+1)L}, \quad (11a)$$

$$\mathbf{H}_k = \begin{bmatrix} h_{k,-L_a} & \dots & 0 \\ \vdots & \ddots & \vdots \\ h_{k,L_h-1} & \dots & h_{k,-L_a} \\ \vdots & \ddots & \vdots \\ 0 & \dots & h_{k,L_h-1} \end{bmatrix} \in \mathbb{R}^{(L_a+L_h+L-1) \times L}, \quad (11b)$$

$$\delta_{\Delta} = \underbrace{[0 \quad \dots \quad 0]}_{L_a} \underbrace{[0 \quad \dots \quad 0]}_{\Delta} \underbrace{[1 \quad 0 \quad \dots \quad 0]}_{L_h+L-1-\Delta}^T \in \mathbb{R}^{L_a+L_h+L-1}, \quad (11c)$$

where \mathbf{H}_k is the convolution matrix of the ReIR for the k -th channel with respect to a chosen reference microphone, with L_a and L_h denoting the length of the anti-causal and causal parts of the ReIR, respectively [16]. α is a real-valued positive amplification factor of the desired speech signal. It should be particularly noted that although the ReIRs are acausal, the control filter \mathbf{w} for reducing noise is still causal.

The solution to (9) is found to be [17]

$$\mathbf{w}_{\text{soft}} = -(\Phi_{\text{rr}} + \mu \mathbf{G}^T \mathbf{H}^T \mathbf{H} \mathbf{G})^{-1} [\Phi - \mu \mathbf{G}^T \mathbf{H}^T (\alpha \delta_{\Delta} - \mathbf{H}\mathbf{q})], \quad (12)$$

where

$$\Phi_{\text{rr}} = \mathbf{G}^T \mathcal{E}\{\mathbf{x}(n)\mathbf{x}^T(n)\} \mathbf{G} + \mathbf{B}, \quad (13a)$$

$$\Phi = \mathbf{G}^T \mathcal{E}\{\mathbf{x}(n)\mathbf{x}^T(n)\} \mathbf{q}. \quad (13b)$$

3.1. Case 1: Matched case (oracle)

To establish a performance bound, we first consider the matched scenario where the secondary path estimate used for optimization exactly matches the physical secondary path. In this case, the control filter in (12) is both optimized and evaluated using the same secondary path. This scenario serves as an oracle performance level and represents an approximate upper bound within the considered formulation.

3.2. Case 2: Mismatched case

In practice, secondary path variations may arise. To analyze the sensitivity of the controlfilter optimization to secondary path mismatch, we consider a set of J secondary path estimates $\{\hat{\mathbf{G}}_j\}_{j=1}^J$, which represent a range of conditions that may or may not accurately characterize the true secondary path \mathbf{G} .

For each estimate, a control filter \mathbf{w}_j is calculated based on the estimate $\hat{\mathbf{G}}_j$ as

$$\mathbf{w}_j = -(\hat{\Phi}_{\text{rr},j} + \mu \hat{\mathbf{G}}_j^T \mathbf{H}^T \mathbf{H} \hat{\mathbf{G}}_j)^{-1} [\hat{\Phi}_j - \mu \hat{\mathbf{G}}_j^T \mathbf{H}^T (\alpha \delta_{\Delta} - \mathbf{H}\mathbf{q})], \quad (14)$$

where the mismatched correlation matrix $\hat{\Phi}_{\text{rr},j}$ and vector $\hat{\Phi}_j$ are constructed according to (13) by replacing \mathbf{G} with $\hat{\mathbf{G}}_j$. The input

correlation matrix remain fixed. Each j -th secondary path estimate was used for optimization and but evaluated on the remaining $J - 1$ paths. This case illustrates the distribution of performance under various degrees of estimate accuracy.

4. CASE 3: ROBUST OPTIMIZATION

Significant secondary path variations can lead to performance degradation when the control filter is optimized for a single nominal secondary path. To ensure consistency across a diverse set of conditions, we propose a robust optimization framework that minimizes the average cost over a set of secondary path estimates.

The objective is to determine a robust control filter $\mathbf{w}_{\text{robust}}$ that minimizes the average cost over the set of J secondary path estimates, which is formulated as

$$\min_{\mathbf{w}} \frac{1}{J} \sum_{j=1}^J \left[\mathcal{E}\{e_j^2(n)\} + \mu \|\mathbf{H}(\mathbf{q} + \hat{\mathbf{G}}_j \mathbf{w}) - \alpha \delta_{\Delta}\|_2^2 \right] + \mathbf{w}^T \mathbf{B} \mathbf{w}, \quad (15)$$

where $e_j(n)$ denotes the inner error microphone signal associated with the j -th secondary path estimate. The robust filter $\mathbf{w}_{\text{robust}}$ can be derived as

$$\mathbf{w}_{\text{robust}} = - \left(\bar{\Phi}_{\text{rr}} + \mu \frac{1}{J} \sum_{j=1}^J \hat{\mathbf{G}}_j^T \mathbf{H}^T \mathbf{H} \hat{\mathbf{G}}_j \right)^{-1} \times \left[\bar{\Phi} - \mu \frac{1}{J} \sum_{j=1}^J \hat{\mathbf{G}}_j^T \mathbf{H}^T (\alpha \delta_{\Delta} - \mathbf{H} \mathbf{q}) \right], \quad (16)$$

where

$$\bar{\Phi}_{\text{rr}} = \frac{1}{J} \sum_{j=1}^J \hat{\mathbf{G}}_j^T \mathcal{E}\{\mathbf{x}(n) \mathbf{x}^T(n)\} \hat{\mathbf{G}}_j + \mathbf{B}, \quad (17a)$$

$$\bar{\Phi} = \frac{1}{J} \sum_{j=1}^J \hat{\mathbf{G}}_j^T \mathcal{E}\{\mathbf{x}(n) \mathbf{x}^T(n)\} \mathbf{q}. \quad (17b)$$

By averaging over the set of secondary path estimates, the robust optimization explicitly accounts for path variations and is expected to reduce sensitivity to mismatch.

5. EVALUATION

5.1. Setup

For the evaluation, we considered a pair of closed-fitting hearables inserted into both ears of a GRAS 45BB-12 KEMAR Head & Torso simulator, as illustrated in Fig. 2a. We used four outer microphones (entrance microphones and concha microphones at the left and right ears, labeled as #1–#4), two inner error microphones (located at the eardrum, labeled as #5 and #6), and the inner drivers acting as the secondary sources. Control was performed independently for each side, using the four outer microphones (#1–#4) in combination with the respective inner error microphone (#5 or #6). The entrance microphones #1 and #3 were chosen as the reference microphones due to the clear speech pickup.

The acoustic scenario (Fig. 2b) was conducted in a moderately reverberant room ($7 \times 6 \times 2.7$ m, $T_{60} \approx 370$ ms). The desired speech source (0° , 0.7 m) consisted of VCTK [19] utterances “005–006” from

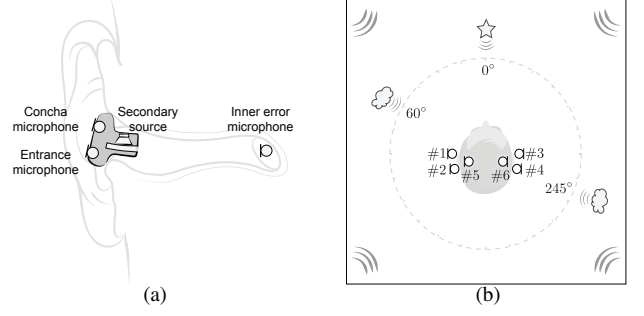


Fig. 2. (a) Illustration of the closed-fitting hearable. (b) Acoustic scenario with one desired speech source at 0° , two noise sources at 60° and 245° , and environmental noise from 12 loudspeakers (omitted for clarity).

speaker “p361”. Two airplane cabin noise sources [20] were positioned at 60° (0.7 m) and 245° (0.9 m). Additionally, a 12-loudspeaker circular array (radius of 1.8 m) generated a diffuse pub scene rendered by TASCAR [21, 22]. All signals were recorded for 10 s at 40 kHz using a dSPACE SCALEXIO LabBox with a field programmable gate array (FPGA). The average leakage signal-to-noise ratio (SNR) at the inner error microphones was -7.0 dB, with -6.6 dB at the left ear and -7.2 dB at the right ear.

The secondary paths for KEMAR were identified by least-squares estimation under white noise excitation. To model secondary path variations, we generated a set of $J = 44$ secondary paths by applying spectral variations derived from human measurements [23, 24] to the KEMAR responses. These variations were converted into causal filters using a windowed inverse Fourier transform and convolved with the KEMAR response. In the simulations, this set of J paths was used to define the three evaluation cases. In Case 1 (Matched), each path was optimized and evaluated on itself, resulting in J scenarios. In Case 2 (Mismatched), each j -th path was used for optimization and evaluated on the remaining $J - 1$ paths, yielding $J(J - 1)$ scenarios in total. In Case 3 (Robust), a single robust filter was optimized using all J paths and evaluated across the same set.

The ReIRs were derived by first obtaining absolute impulse responses from the desired source to all microphones via exponential sine sweep (ESS). A least-squares estimation, using white noise as a synthetic excitation, was then applied to identify the ReIRs with respect to the reference microphone.

The lengths of the control filters and secondary paths were set to $L_w = 1800$ and $L_g = 1800$, respectively, while ReIR modeling lengths were $L_a = L_h = 4500$. The desired speech delay was $\Delta = 240$ (6 ms). Internal processing latencies of 2 and 3 samples from the dSPACE system were incorporated for the feedforward and feedback paths, respectively. The amplification factor for the desired speech was set to $\alpha = 2.0$. To ensure stability, the regularization parameters were chosen relative to the largest eigenvalue (λ_{max}) of the input correlation matrix. In particular, the feedforward regularization parameter was set to $\beta_{\text{FF}} = \lambda_{\text{max}}/10^4$. The feedback channel generally needs more regularization to prevent instability, and thus $\beta_{\text{FB}} = 30 \beta_{\text{FF}}$ was used. The trade-off parameter μ was varied from 1 to 3000, which corresponds to a $\log_{10}(\mu)$ range of 0 to 3.48, to evaluate the performance.

5.2. Evaluation metrics

The performance was evaluated in terms of noise reduction, speech distortion, speech quality and intelligibility.

The noise reduction is defined as the difference between the power

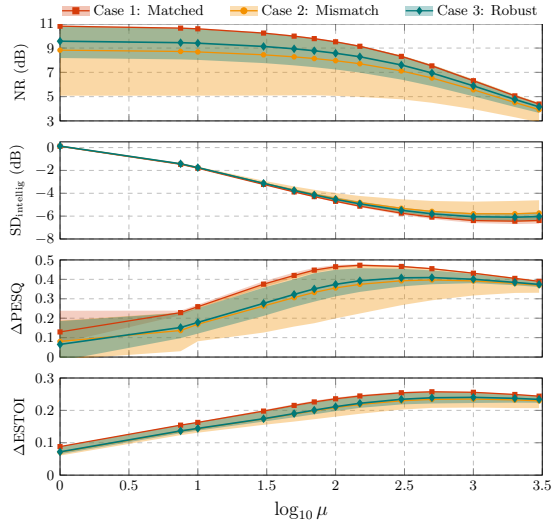


Fig. 3. Noise reduction, intelligibility-weighted spectral distortion, narrowband PESQ improvement, and ESTOI improvement for the matched case (Case 1), the mismatched case (Case 2), and the robust case (Case 3) at the right inner error microphone (#6) with respect to different values of the trade-off parameter μ . Solid lines denote the mean across scenarios, and the shaded regions indicate the 5th–95th percentile range.

of the noise component of the leakage $p_v(n)$ (without control) and the noise component of the inner error microphone signal $e_v(n)$ (with control), i.e.,

$$\text{NR (dB)} = 10 \log_{10} \sum_{n=1}^N p_v^2(n) - 10 \log_{10} \sum_{n=1}^N e_v^2(n), \quad (18)$$

where N denotes the total signal length.

The intelligibility-weighted spectral distortion is used to assess the amount of speech distortion [8, 25, 26]. It is defined as

$$\text{SD}_{\text{intellig}} \text{ (dB)} = \sum_{b=1}^{\mathcal{B}} I(\omega_b) 10 \log_{10} \frac{\mathcal{P}_\epsilon(\omega_b)}{\mathcal{P}_{\text{ref},s}(\omega_b)}, \quad (19)$$

where the band importance function $I(\omega_b)$ expresses the importance of the b -th one-third octave band for intelligibility [27], and \mathcal{B} denotes the total number of bands. $\mathcal{P}_\epsilon(\omega_b)$ is the power spectral density of $\epsilon(n)$ in the b -th band, where $\epsilon(n) = e_s(n) - \alpha x_{\text{ref},s}(n - \Delta)$. $\mathcal{P}_{\text{ref},s}(\omega_b)$ is the power spectral density of $\alpha x_{\text{ref},s}(n - \Delta)$ in the b -th band.

In addition, we considered the narrowband perceptual evaluation of speech quality (PESQ) [28] and the extended short-term objective intelligibility (ESTOI) [29] metrics using $\alpha x_{\text{ref},s}(n - \Delta)$ as the reference signal. We evaluated the PESQ and ESTOI differences between the leakage (without control) and the inner error microphone signal (with control).

5.3. Simulation results

The performance of the three cases is illustrated in Fig. 3 for the right inner error microphone (#6). The solid lines denote the mean performance across all evaluated scenarios, while the shaded regions indicate the 5th–95th percentile range. The same trends were observed at the left ear (#5) and are omitted for brevity.

The matched case achieves the best mean performance overall in terms of noise reduction, speech distortion, PESQ improvement, and ESTOI improvement across the entire range of μ , while exhibiting only

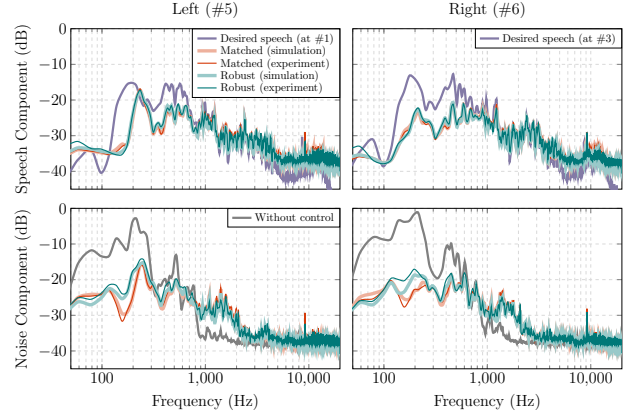


Fig. 4. Spectra of the speech component (top row) and the noise component (bottom row) of the inner error microphone signals (#5 and #6) from the simulated and experimental evaluations for the matched and the robust cases for $\mu = 150$, i.e., $\log_{10}(\mu) = 2.18$.

a narrow spread. This serves as the upper bound as expected. In contrast, the mismatched case shows a substantially wider performance range, particularly for noise reduction, where the 5th–95th percentile interval spans up to approximately 6 dB. The PESQ improvement also exhibits a noticeably larger spread, whereas the speech distortion and ESTOI improvement are less affected by the mismatch. The proposed robust case (Case 3) achieves a mean performance slightly lower than the matched case but comparable to the mismatched case, while significantly narrowing the 5th to 95th percentile range to mitigate the impact of secondary path variations across the entire range of μ .

5.4. Experimental validation

To validate the simulation results, we implemented the control filters obtained from the matched and robust optimizations on the real-time dSPACE system in the same acoustic scenario. The control filter for the matched case was calculated according to (12) using the matched secondary path from KEMAR, and the filter for the robust case was calculated according to (16) using the average matrices across all 44 paths. The spectra of the speech and noise components at the error microphones for $\mu = 150$ ($\log_{10}(\mu) \approx 2.18$) are shown in Fig. 4. The experimental and simulation results are consistent, thus validating the simulation findings.

6. CONCLUSION

This paper examined the impact of secondary path variations on the performance of spatially selective active noise control systems for hearables. Simulation results showed that the matched case, assuming oracle knowledge of the secondary path, achieves the best overall performance. However, when the estimated secondary path does not match the true secondary path, the performance can degrade substantially, particularly in terms of noise reduction. To address this issue, we proposed a robust optimization framework that minimizes the average cost over a set of secondary path estimates. The resulting robust filter achieves performance that is slightly lower than that of the matched case but remains stable across different secondary path conditions. Compared with filters optimized for a single mismatched secondary path, the proposed robust filter produces more consistent performance across the considered set of secondary path estimates. Experimental results obtained with a real-time system are consistent with the simulation findings.

7. REFERENCES

- [1] S. M. Kuo and D. R. Morgan, *Active noise control systems: Algorithms and DSP implementations*. Wiley, 1996.
- [2] S. J. Elliott, *Signal processing for active control*. Academic Press, 2000.
- [3] C. Hansen, S. Snyder, X. Qiu, L. Brooks, and D. Moreau, *Active control of noise and vibration*, 2nd ed. CRC Press, Nov. 2012.
- [4] P. R. Benois, R. Roden, M. Blau, and S. Doclo, "Optimization of a fixed virtual sensing feedback ANC controller for in-ear headphones with multiple loudspeakers," in *Proc. IEEE International Conference on Acoustics, Speech and Signal Processing (ICASSP)*, Singapore, 2022, pp. 8717–8721.
- [5] F. Hilgemann, E. Chatzimoustafa, and P. Jax, "Data-driven uncertainty modeling for robust feedback active noise control in headphones," *Journal of the Audio Engineering Society*, vol. 72, no. 12, pp. 873–883, Apr 2024.
- [6] C.-Y. Chang, A. Siswanto, C.-Y. Ho, T.-K. Yeh, Y.-R. Chen, and S. M. Kuo, "Listening in a noisy environment: Integration of active noise control in audio products," *IEEE Consumer Electronics Magazine*, vol. 5, no. 4, pp. 34–43, 2016.
- [7] R. Gupta, J. He, R. Ranjan, W.-S. Gan, F. Klein, C. Schneiderwind, A. Neidhardt, K. Brandenburg, and V. Välimäki, "Augmented/mixed reality audio for hearables: Sensing, control, and rendering," *IEEE Signal Processing Magazine*, vol. 39, no. 3, pp. 63–89, 2022.
- [8] R. Serizel, M. Moonen, J. Wouters, and S. H. Jensen, "Integrated active noise control and noise reduction in hearing aids," *IEEE Transactions on Audio, Speech, and Language Processing*, vol. 18, no. 6, pp. 1137–1146, 2010.
- [9] D. Dalga and S. Doclo, "Influence of secondary path estimation errors on the performance of ANC-motivated noise reduction algorithms for hearing aids," in *Proc. IEEE Workshop on Applications of Signal Processing to Audio and Acoustics (WASPAA)*, New Paltz, USA, 2013, pp. 1–4.
- [10] V. Patel, J. Cheer, and S. Fontana, "Design and implementation of an active noise control headphone with directional hear-through capability," *IEEE Transactions on Consumer Electronics*, vol. 66, no. 1, pp. 32–40, Feb. 2020.
- [11] T. Xiao, B. Xu, and C. Zhao, "Spatially selective active noise control systems," *The Journal of the Acoustical Society of America*, vol. 153, no. 5, pp. 2733–2744, May 2023.
- [12] B. Van Veen and K. Buckley, "Beamforming: A versatile approach to spatial filtering," *IEEE ASSP Magazine*, vol. 5, no. 2, pp. 4–24, 1988.
- [13] S. Gannot, E. Vincent, S. Markovich-Golan, and A. Ozerov, "A consolidated perspective on multimicrophone speech enhancement and source separation," *IEEE/ACM Transactions on Audio, Speech, and Language Processing*, vol. 25, no. 4, pp. 692–730, 2017.
- [14] S. Doclo, W. Kellermann, S. Makino, and S. E. Nordholm, "Multichannel signal enhancement algorithms for assisted listening devices: Exploiting spatial diversity using multiple microphones," *IEEE Signal Processing Magazine*, vol. 32, no. 2, pp. 18–30, Mar. 2015.
- [15] T. Xiao and S. Doclo, "Effect of target signals and delays on spatially selective active noise control for open-fitting hearables," in *Proc. IEEE International Conference on Acoustics, Speech and Signal Processing (ICASSP)*, Seoul, Republic of Korea, 2024, pp. 1056–1060.
- [16] ———, "Spatially selective active noise control for open-fitting hearables with acausal optimization," in *Proc. Forum Acusticum EuroNoise 2025*, Málaga, Spain, Jun. 2025, pp. 117–124.
- [17] T. Xiao, R. Roden, M. Blau, and S. Doclo, "Soft-constrained spatially selective active noise control for open-fitting hearables," in *Proc. IEEE Workshop on Applications of Signal Processing to Audio and Acoustics (WASPAA)*, Tahoe City, USA, 2025, pp. 1–5.
- [18] H. Schepker, F. Denk, B. Kollmeier, and S. Doclo, "Robust single- and multi-loudspeaker least-squares-based equalization for hearing devices," *EURASIP Journal on Audio, Speech, and Music Processing*, vol. 2022, no. 1, pp. 1–14, 2022.
- [19] C. Veaux, J. Yamagishi, and K. MacDonald, "CSTR VCTK corpus: English multi-speaker corpus for CSTR voice cloning toolkit," 2017. [Online]. Available: <https://doi.org/10.7488/ds/2645>
- [20] British Broadcasting Corporation, "Sound sample 07025055," BBC Sound Effects Archive, 2024, accessed: March 04, 2026. [Online]. Available: <https://sound-effects.bbcrewind.co.uk/search?q=07025055>
- [21] G. Grimm, J. Luberadzka, and V. Hohmann, "A toolbox for rendering virtual acoustic environments in the context of audiology," *Acta acustica united with acustica*, vol. 105, no. 3, pp. 566–578, 2019.
- [22] G. Grimm, M. Hendrikse, and V. Hohmann, "Pub environment," Sep. 2021. [Online]. Available: <https://doi.org/10.5281/zenodo.5886987>
- [23] F. Denk, M. Lettau, H. Schepker, S. Doclo, R. Roden, M. Blau, J.-H. Bach, J. Wellmann, and B. Kollmeier, "A one-size-fits-all earpiece with multiple microphones and drivers for hearing device research," in *Proc. AES International Conference on Headphone Technology*, San Francisco, USA, Aug. 2019, pp. 1–9.
- [24] F. Denk and B. Kollmeier, "The hearpiece database of individual transfer functions of an in-the-ear earpiece for hearing device research," *Acta Acustica*, vol. 5, no. 2, pp. 1–16, 2021.
- [25] A. Spriet, M. Moonen, and J. Wouters, "Spatially pre-processed speech distortion weighted multi-channel Wiener filtering for noise reduction," *Signal Processing*, vol. 84, no. 12, pp. 2367–2387, 2004.
- [26] S. Doclo, A. Spriet, J. Wouters, and M. Moonen, "Frequency-domain criterion for the speech distortion weighted multichannel Wiener filter for robust noise reduction," *Speech Communication*, vol. 49, no. 7, pp. 636–656, 2007.
- [27] Acoustical Society of America (ASA), "Methods for Calculation of the Speech Intelligibility Index," American National Standards Institute (ANSI), ANSI/ASA S3.5-1997 Standard, 1997.
- [28] A. Rix, J. Beerends, M. Hollier, and A. Hekstra, "Perceptual evaluation of speech quality (PESQ)—a new method for speech quality assessment of telephone networks and codecs," in *Proc. IEEE International Conference on Acoustics, Speech, and Signal Processing. Proceedings (ICASSP)*, Salt Lake City, USA, May 2001, pp. 749–752.
- [29] J. Jensen and C. H. Taal, "An algorithm for predicting the intelligibility of speech masked by modulated noise maskers," *IEEE/ACM Transactions on Audio, Speech, and Language Processing*, vol. 24, no. 11, pp. 2009–2022, 2016.